Dosimetry of ^{177}Lu-PSMA-617 in Metastatic Castration-Resistant Prostate Cancer: Correlations Between Pretherapeutic Imaging and Whole-Body Tumor Dosimetry with Treatment Outcomes

John Violet[1], Price Jackson[1,2], Justin Ferdinandus[2], Shahneen Sandhu[3], Tim Akhurst[2], Amir Iravani[2], Grace Kong[2], Aravind Ravi Kumar[2], Sue Ping Thang[2], Peter Eu[2], Mark Scalzo[2], Declan Murphy[4,5], Scott Williams[1,5], Rodney J. Hicks[2,5], and Michael S. Hofman[2,5]

[1]Department of Radiation Oncology, Peter MacCallum Cancer Centre, Melbourne, Australia; [2]Department of Molecular Imaging, Peter MacCallum Cancer Centre, Melbourne, Australia; [3]Department of Medical Oncology, Peter MacCallum Cancer Centre, Melbourne, Australia; [4]Department of Uro-Oncology, Peter MacCallum Cancer Centre, Melbourne, Australia; and [5]Sir Peter MacCallum Department of Oncology, University of Melbourne, Melbourne, Australia

[177]Lu-prostate-specific membrane antigen (PSMA)–617 enables targeted delivery of β-particle radiation to prostate cancer. We determined its radiation dosimetry and relationships to pretherapeutic imaging and outcomes. **Methods:** Thirty patients with prostate cancer receiving ^{177}Lu-PSMA-617 within a prospective clinical trial (ACTRN12615000912583) were studied. Screening ^{68}Ga-PSMA-11 PET/CT demonstrated high PSMA expression in all patients. After therapy, patients underwent quantitative SPECT/CT at 4, 24, and 96 h. Pharmacokinetic uptake and clearance at a voxel level were calculated and translated into absorbed dose using voxel S values. Volumes of interest were drawn on normal tissues and tumor to assess radiation dose, and a whole-body tumor dose was defined. Correlations between PSMA PET/CT parameters, dosimetry, and biochemical and therapeutic response were analyzed to identify relationships between absorbed dose, tumor burden, and patient physiology. **Results:** Mean absorbed dose to kidneys, submandibular and parotid glands, liver, spleen, and bone marrow was 0.39, 0.44, 0.58, 0.1, 0.06, and 0.11 Gy/MBq, respectively. Median whole-body tumor-absorbed dose was 11.55 Gy and correlated with prostate-specific antigen (PSA) response at 12 wk. A median dose of 14.1 Gy was observed in patients achieving a PSA decline of at least 50%, versus 9.6 Gy for those achieving a PSA decline of less than 50% ($P < 0.01$). Of 11 patients receiving a tumor dose of less than 10 Gy, only one achieved a PSA response of at least 50%. On screening PSMA PET, whole-body tumor SUV_{mean} correlated with mean absorbed dose ($r = 0.62$), and SUV_{max} of the parotids correlated with absorbed dose ($r = 0.67$). There was an inverse correlation between tumor volume and mean dose to the parotids ($r = -0.41$) and kidneys ($r = -0.43$). The mean parotid dose was also reduced with increasing body mass ($r = -0.41$) and body surface area ($r = -0.37$). **Conclusion:** ^{177}Lu-PSMA-617 delivers high absorbed doses to tumor, with a significant correlation between whole-body tumor dose and PSA response. Patients receiving less than 10 Gy were unlikely to achieve a fall in PSA of at least 50%. Significant correlations between aspects of screening ^{68}Ga-PET/CT and tumor and normal tissue dose were observed, providing a rationale for patient-specific dosing. Reduced salivary and kidney doses were observed in patients with a higher tumor burden. The parotid dose also reduced with increasing body mass and body surface area.

Key Words: ^{177}Lu-PSMA-617; dosimetry; prostate cancer; theranostics; radionuclide therapy

Prostate-specific membrane antigen (PSMA) is a type II transmembrane protein expressed in most clinically significant prostate cancers. Its expression increases in higher-grade, metastatic, and androgen-insensitive tumors (*1–5*), whereas expression is largely absent in benign or hyperplastic prostate tissue (*6*). Lower PSMA expression occurs in proximal small bowel, kidneys, and salivary and lacrimal glands (*7,8*). PSMA is a favorable target for molecular imaging (*9–14*) and therapy (*15–21*) of prostate cancer labeled with positron and β-emitting radionuclides, respectively

Radiolabeled small-molecule inhibitors of PSMA show promise as therapeutic agents in advanced prostate cancer (*22*), and understanding their radiation dosimetry is key to their development. [177]Lu has favorable decay characteristics for radionuclide therapy, possessing both a short-range cytotoxic β-particle and a small γ-emission–enabling biodistribution to be quantified using scintigraphy.

Dosimetric estimates from retrospective series with β-labeled small molecules suggest that the normal tissues receiving the highest absorbed doses are small intestine, kidneys, and salivary glands (*15,23–28*).

Tumor dose may be an important predictor of clinical response, but estimation of a clinically relevant tumor-absorbed dose is challenging in patients with multiple sites of disease, often with variable uptake and retention of the therapeutic agent. It is difficult to envisage how index lesion dosimetry, as is commonly performed, can reflect this heterogeneity. In a novel approach we have estimated mean "total-body" tumor dose, alongside lesional tumor dosimetry, postulating that this may be more clinically relevant.
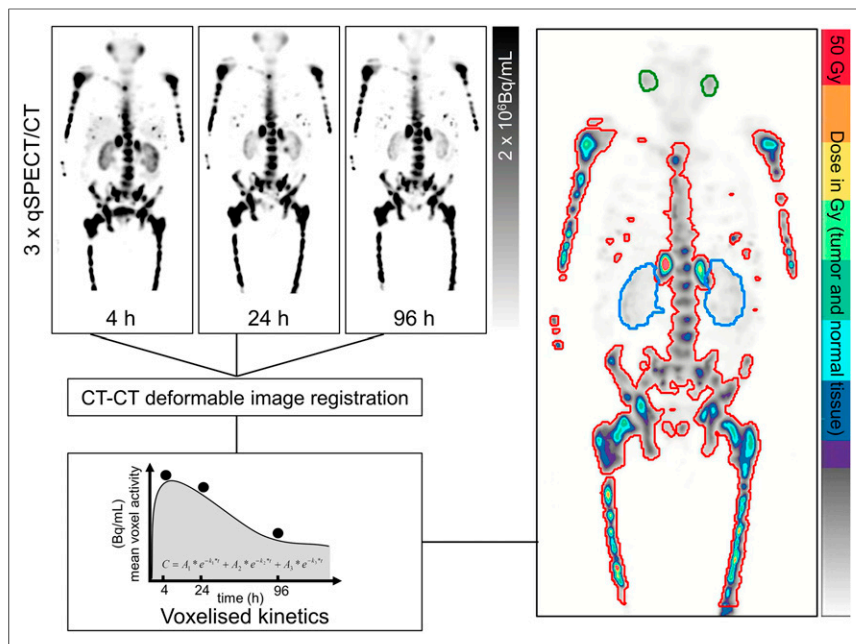
FIGURE 1. Schematic of voxel-based dosimetry workflow, showing regions of interest for whole-body tumor volume (red), kidneys (blue), and salivary glands (green). qSPECT/CT = quantitative SPECT/CT.

The primary aim of this study was to perform radiation dosimetry in men with advanced prostate cancer treated in a prospective clinical trial (*29*) using an automated voxelized dosimetry tool (*30*). We evaluated whether pretherapeutic ^{68}Ga-PSMA PET is a predictor of absorbed dose, whether a "sink effect" was evident, and whether dose in normal tissues and tumor can predict toxicity and clinical response.

MATERIALS AND METHODS

Study Design and Patient Population

Between August 2015 and December 2016, 30 patients with PSMA-avid metastatic castration-resistant prostate cancer were enrolled and underwent up to 4 cycles of ^{177}Lu-PSMA-617. Sufficient PSMA avidity for therapy was defined on ^{68}Ga-PSMA-11 PET/CT as at least 1 site of metastatic disease with intensity significantly greater than normal liver (SUV_{max} at least 1.5 times SUV of normal liver). ^{18}F-FDG PET/CT scans excluded patients if sites of ^{18}F-FDG–positive disease without high PSMA expression were identified. Disease progression, either radiologically or clinically, was mandated before entry into

the trial. The study protocol was approved by the institutional ethics board and was conducted in accordance with the declaration of Helsinki and good clinical practice. The trial was registered with the Australian New Zealand Clinical Trials Registry (ANZCTR12615000912583), and all patients gave written informed consent before study entry.

The ^{177}Lu-PSMA-617 preparation, study design, and procedures have been previously described (*29*). The administered radioactivity (GBq) was adjusted according to tumor burden, patient weight, and renal function adapted from our practice using ^{177}Lu-DOTATATE as follows. Activity was increased by 1 GBq if there were more than 20 sites of disease, decreased by 1 GBq if fewer than 10 sites, increased by 0.5 GBq per factor if weight was more than 90 kg or glomerular filtration rate more than 90 mL/min, and decreased by 0.5 GBq if weight was less than 70 kg or glomerular filtration rate less than 60 mL/min. Up to 4 cycles of therapy were administered at 6 weekly intervals.

Image Acquisition and Dosimetry

Thirty dosimetric image sets were obtained after initial therapy with serial quantitative SPECT/CT (2- or 3-bed-position acquisition) encompassing neck to pelvis performed 4, 24, and 96 h after injection (Symbia T6 or Intevo 16; Siemens A.G.) (Fig. 1).

SPECT voxels were acquired with dimensions of 4.8 × 4.8 × 4.8 mm, and ^{177}Lu activity was quantified by conversion of voxel counts per seconds to activity per unit volume using attenuation, scatter, and dead-time corrections according to the protocol described by Beauregard et al. (*31*). Serial quantitative SPECT images were converted into voxel dose maps using a modified methodology described previously (*30*). Images were aligned by sequential rigid and B-spline deformable registration with Elastix (version 4.8) (*32*) using a weighted normalized correlation metric (80%) with transform bending energy penalty (20%). CT-to-CT registration was used to compute deformation fields for alignment of fused SPECT volumes. Images were resampled to 3 × 3 × 3 mm³ voxels to assist with voxel S-value convolution. Time–activity curves were independently calculated in each voxel based on a 3-phase exponential clearance model yielding 3-dimensional cumulated activity maps (*30*). Dose conversion was performed by convolving GATE-derived voxel dose kernel (maximum

TABLE 1
Absorbed Doses in Normal Tissues (Gy) and Dose per Administered Activity (Gy/GBq) Following First
Cycle of Therapy (Voxelized Technique)

Target organ	Median dose	Mean dose	Minimum dose	Maximum dose	SD
Parotid glands	4.0 (0.48)	4.8 (0.58)	1.12 (0.13)	15.5 (1.87)	3.58 (0.43)
Submandibular glands	3.2 (0.38)	3.7 (0.44)	0.20 (0.02)	14.50 (1.75)	2.95 (0.36)
Lacrimal glands	2.7 (0.32)	2.8 (0.36)	0.8 (0.10)	6.0 (0.81)	1.33 (0.18)
Kidneys	3.1 (0.38)	3.2 (0.39)	0.77 (0.09)	7.0 (0.84)	1.28 (0.15)
Spleen	0.5 (0.06)	0.7 (0.08)	0.24 (0.03)	3.16 (0.38)	0.53 (0.06)
Liver	0.7 (0.08)	0.8 (0.10)	0.30 (0.04)	2.60 (0.31)	0.44 (0.05)
Marrow	0.8 (0.10)	1.0 (0.11)	0.10 (0.01)	2.80 (0.34)	0.80 (0.10)

	Voxel technique				MIRD sphere model			
Site	Mean dose	Minimum dose	Maximum dose	SD	Mean dose	Minimum dose	Maximum dose	SD
Lacrimal	2.77 (0.36)	0.80 (0.10)	6.0 (0.81)	1.33 (0.18)	28.65 (3.78)	10.01 (1.19)	76.28 (9.19)	16.39 (2.13)
Submandibular	3.66 (0.44)	0.20 (0.02)	14.5 (1.75)	2.95 (0.36)	5.03 (0.67)	1.14 (0.17)	13.42 (2.0)	3.25 (0.45)
Parotid	4.78 (0.58)	1.12 (0.13)	15.5 (1.87)	3.58 (0.43)	4.82 (0.64)	0.63 (0.08)	14.70 (2.23)	3.14 (0.46)

range, 40 mm) based on decay of ^{177}Lu in ICRP soft tissue (33). Dose volumes were saved in DICOM format and contoured on clinical workstations. Regions of interest were drawn in normal tissues and tumor to determine absorbed dose. Mean "whole-body" tumor volume was determined by applying a 5-Gy threshold to the voxel dose volumes and then removing regions of physiologic uptake.

For normal tissues with a small size, namely the salivary and lacrimal glands, expanded contours encompassing the organs plus a 1- to 2-cm margin were also determined. Lacrimal dosimetry could not be obtained in 15 patients, as they were not included in the SPECT field of view at all 3 of the time points. These volumes were used to compute regional activity at each time point, and cumulated activity was converted to absorbed dose using the OLINDA sphere model S values, adjusted for patient-specific volumes defined on pretreatment ^{68}Ga-PSMA PET scans (34–36). The duodenum presents a logistic challenge for our automated system because of its motile nature, and dosimetry for this organ has not been determined.

^{68}Ga-PSMA PET/CT Analyses

Baseline ^{68}Ga-PSMA-11 PET/CT was used to assess eligibility for treatment. "Whole-body" tumor volume was determined using an automated threshold encompassing activity with an SUV greater than 3, with removal of areas of physiologic uptake (MIM Software). This tumor volume was further subdivided into bone and soft tissue using subthresholding to 100 Hounsfield units and visual adjustment

FIGURE 2. Correlation between SUV$_{max}$ in parotid glands on screening ^{68}Ga-PSMA PET and absorbed dose.

of the contours. Salivary glands were contoured on the PET sequence using an edge detection algorithm (PET Edge; MIM Software). For each volume of interest, the SUV$_{max}$, SUV$_{mean}$, and volume were calculated.

Statistical Analysis

All continuous data are expressed as the median, SD, and range and R-statistics. We calculated correlations between parameters of PSMA PET/CT and dosimetric results estimated using our voxel-based method. We computed Spearman r and P values for each correlation and tested for difference in absorbed doses to tumor in patients achieving a prostate-specific antigen (PSA) response greater than 50% using a Wilcoxon–Mann–Whitney test. All analyses were conducted with R (R Development Team, 2018), and P values of less than 0.05 were considered statistically significant.

RESULTS

Baseline characteristics of patients and administered activities were documented (Supplemental Appendix 1). The median age of subjects was 70.5 y (interquartile range, 67–75 y), and patients had a median PSA doubling time of 2.4 mo. All patients were heavily pretreated, with 87% receiving prior systemic chemotherapy; 47% had also received second-line chemotherapy. Eighty-three percent had received second-generation antiandrogens, and more than 90% had more than 20 sites of disease. The mean administered activity was 7.8 GBq (range, 5.7–8.7 GBq).

Normal-Organ Dosimetry

Dosimetric estimates in parotid and submandibular glands, kidneys, spleen, liver, and noninfiltrated bone marrow are summarized in Tables 1 and 2. Salivary glands, lacrimal glands, and kidneys received the highest absorbed doses. For lacrimal glands, the application of MIRD yielded doses higher by a factor of 10 than the voxel technique; these are shown in Table 2.

SUV$_{max}$ of parotid glands on ^{68}Ga-PSMA-11 PET correlated with mean absorbed dose (Gy/GBq) from voxel-based dosimetry ($r = 0.68$, $P < 0.01$) and is shown in Figure 2. There was an inverse correlation between tumor volume (defined on PSMA PET) and mean dose to the parotid glands ($r = -0.41$, $P = 0.03$) and kidneys ($r = -0.43$; $P = 0.02$). Mean parotid absorbed dose decreased with increasing body mass ($r = -0.41$, $P < 0.01$) and body surface area ($r = -0.37$, $P < 0.05$) and is shown in Figure 3. There was no significant correlation between parotid dose and glomerular filtration rate ($r = 0.13$, $P = 0.5$).

Tumor Dosimetry

Absorbed whole-body tumor doses are shown in Table 3 and further divided into tumor-bearing bone and lymph/visceral regions.
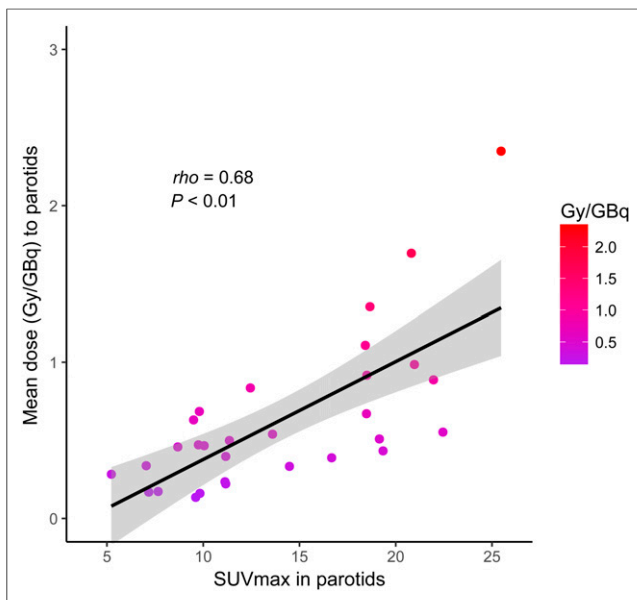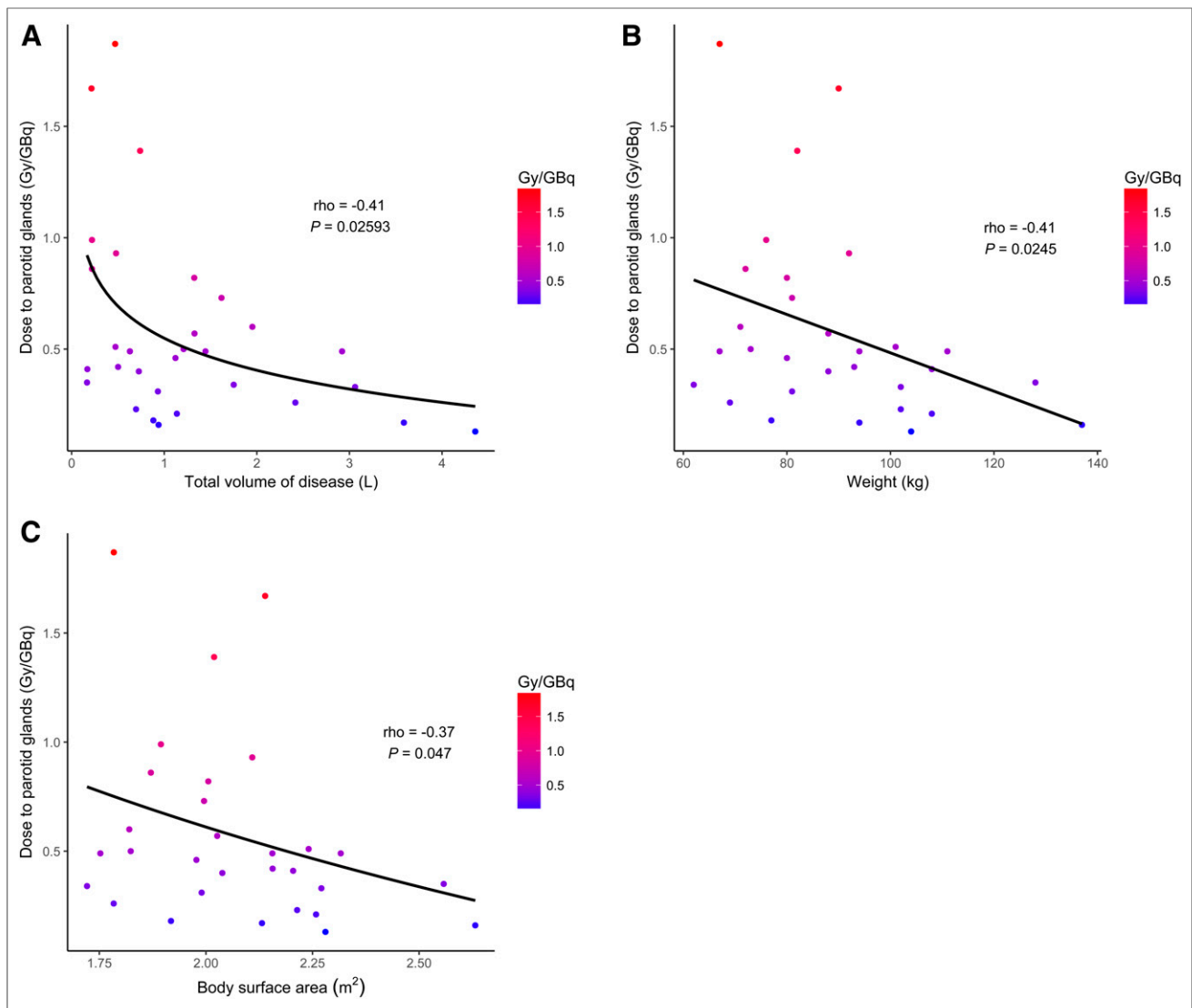
FIGURE 3. (A) Correlation between tumor volume on screening ^{68}Ga-PSMA PET and mean parotid absorbed dose. (B) Correlation between body mass and mean parotid absorbed dose. (C) Correlation between body surface area and mean parotid absorbed dose.

"Whole-body" tumor dose was associated with PSA response at 12 wk, with a median dose of 14.1 Gy (mean, 14.7 Gy; SD, 3.9 Gy; range, 9.7–24.4 Gy) in patients achieving a PSA decline of at least 50%, versus 9.6 Gy (mean, 10.4 Gy; SD, 3.4 Gy; range, 7.3–20.3 Gy) for those achieving a PSA decline of less than 50% ($P < 0.01$), and is shown in Figure 4A. With a tumor dose of less than 10 Gy, only 1 patient achieved a PSA decline of at least 50% and 10 patients had a PSA decline of less than 50%. Nonresponding patients

achieved a significantly lower tumor dose than responders ($P < 0.01$) (Supplemental Fig. 1; supplemental materials are available at http://jnm.snmjournals.org). Maximum tumor-absorbed dose in index lesions did not correlate with PSA response at 12 wk and is shown in Figure 4B.

We found a significant correlation between the SUV$_{mean}$ of "whole-body" tumor on screening ^{68}Ga-PSMA PET and the "whole-body dose" (Gy/GBq) ($r = 0.62$, $P < 0.01$); these correlations are

TABLE 3
Maximum Absorbed Dose (Gy) and Dose per Administered Activity (Gy/GBq) in Tumor-Bearing Bone, Lymph Nodes, and Mean Whole-Body Tumor Doses Above 5 Gy

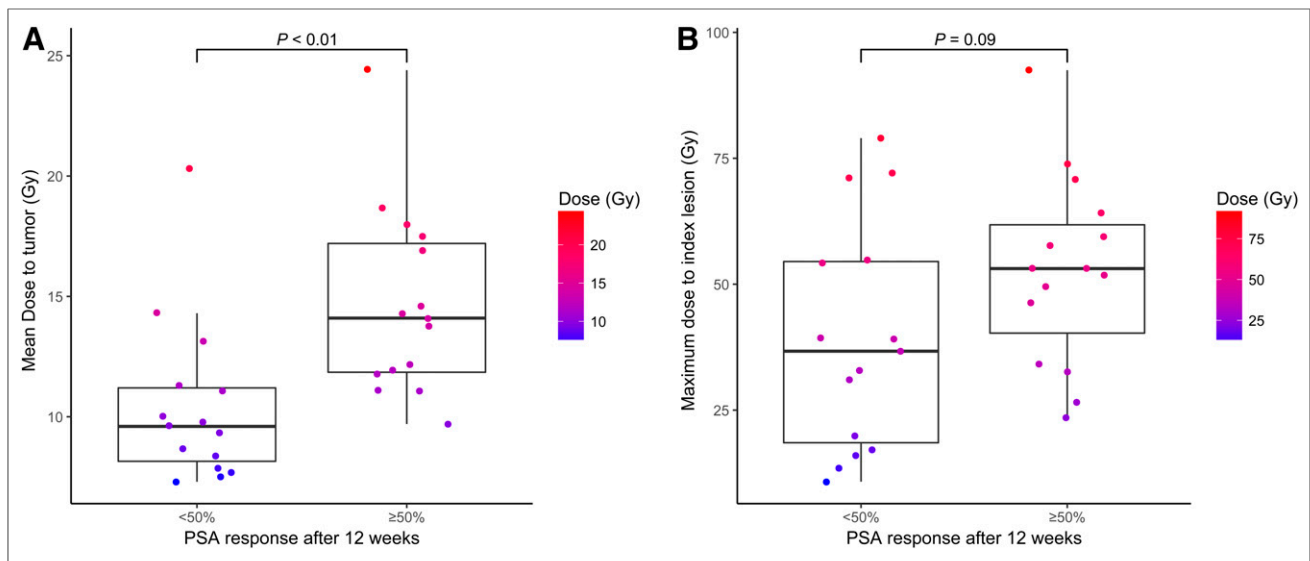| Tumor site	Median dose	Mean dose	Range	SD
Bone	39.2	41.0 (5.28)	3.4–73.9 (0.41–10.71)	18.88 (2.46)
Node	17.5	28.79 (3.91)	4.4–92.5 (0.52–16.23)	25.13 (3.93)
Mean whole-body dose > 5 Gy	11.55	12.55	7.3–24.4	4.18

FIGURE 4 (A) Mean whole-body tumor-absorbed dose was significantly higher in patients achieving greater than 50% fall in serum PSA at 12 wk. (B) Maximum tumor-absorbed dose in index lesions was not significantly different in patients achieving greater than 50% fall in serum PSA at 12 wk.

shown in Figure 5. Both soft-tissue and bone metastases separately showed a significant correlation between SUV_{mean} and mean absorbed dose ($r = 0.55$, $P < 0.01$, and $r = 0.60$, $P < 0.01$), respectively. There was a trend for a higher SUV_{mean} to be associated with a PSA response at 12 wk, with a median SUV_{mean} of 8.9 (mean, 9.2; SD, 2.8; range, 5.3–15.6) in patients achieving a decline of at least 50%, versus 7.0 (mean, 7.3; SD, 1.9; range, 5.1–12.1) in those who did not ($P = 0.056$) (Supplemental Fig. 2).

DISCUSSION

We have demonstrated high tumor–to–normal-tissue uptake with prolonged retention of radionuclide in tumor-bearing areas in men with metastatic prostate cancer treated with ^{177}Lu-PSMA-617.
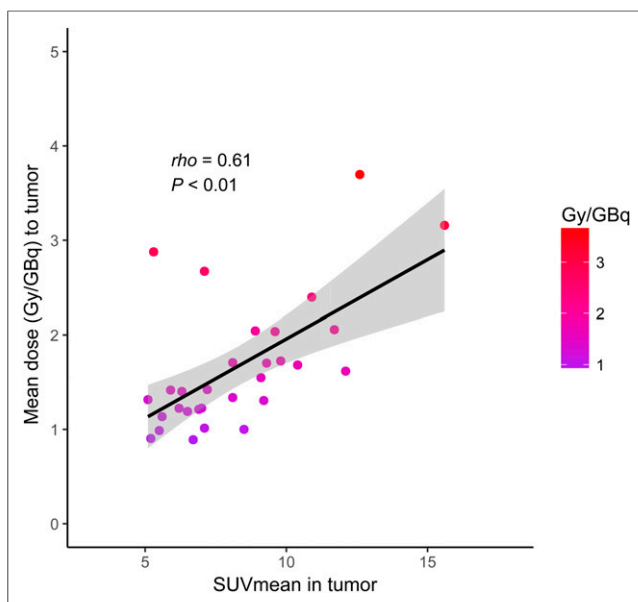

FIGURE 5. Correlation between SUV_{mean} on screening ^{68}Ga-PSMA PET and mean whole-body tumor dose calculated using 5-Gy dose cutoff.

Previous studies have generally used whole-body planar scintigraphy to measure activity (Supplemental Appendix 2) and may overestimate activity, particularly if significant activity overlies organs or tumor-bearing regions of interest. This overestimation has been well described in renal dosimetry after therapy using radiolabeled somatostatin analogs (37,38) and is relevant in PSMA radionuclide therapy, where bowel and liver may overlie kidneys and bone metastases may overlie salivary and lacrimal glands (13,24). The drawing of regions of interest on multiple sequential planar images is also time-consuming and subject to interobserver variation.

Although widely used, MIRD has several limitations as a dosimetry tool. Developed for population-based dosimetry, it assumes that organ masses and shapes conform to those of a standard man. Furthermore, it does not provide conversion factors for tumor or all organs, with no S factors for lacrimal or salivary glands. To assess dose in these organs using MIRD, we applied the OLINDA sphere model using volumes taken from pretreatment ^{68}Ga-PSMA PET scans (36). These structures also present challenges for our voxelized dosimetry technique because of partial-volume effects and a greater likelihood of potential misregistration. The latter is most notable in the head and neck, where head rotation may occur between scans (35–39), and is of particular concern defining very small ROIs, such as lacrimal glands.

Absorbed dose estimates using both the voxel-based technique and MIRD show broad agreement for salivary tissues (24–27). For lacrimal glands, however, MIRD dose was higher by a factor of 10 than the voxel dose. Because of their small size, which presents challenges for both methods, the actual absorbed dose likely lies somewhere between their respective estimates. Some dosimetry studies suggest that lacrimal glands may be dose-limiting (23,26), whereas in clinical practice significant lacrimal toxicity is rare (29).

In our study, the highest doses occurred in salivary glands, lacrimal glands, and kidneys. Median renal doses were slightly lower than those predicted by others, perhaps reflecting overlying bowel or liver activity. Salivary gland doses are in the lower range of the published series, perhaps relating to overlying activity in bone or partial-volume

effects of the voxelized technique. Liver and spleen doses are similar to those reported by Delker et al., who also used SPECT/CT to derive their activity maps (24). Regardless, all the available SPECT data suggest that these organs are not dose-limiting.

Our dosimetry suggests it is safe to deliver multiple cycles of therapy before exceeding the tolerance of salivary glands and kidneys. Assuming average biodistribution after 4 cycles of therapy at an administered activity of 8 GBq, doses to kidneys are 12.5 Gy, lacrimal glands 11.5 Gy, parotid glands 18.6 Gy, and submandibular glands 14.1 Gy. These doses meet accepted standards used in external-beam radiotherapy of 15–18 Gy (40), 34 Gy (41), and 20–25 Gy (salivary tissues) (42). It is well known that normal tissues can tolerate higher absorbed doses following radionuclide therapy than external beam (43) and is explained by the linear-quadratic formula developed following years of use in fractionated external-beam radiotherapy (44). Radiobiologic modeling, for example, suggests that renal tolerance following radionuclide therapy will be almost twice that expected following external beam (15).

Following 4×8 GBq, we would predict a marrow dose of 3.5 Gy, a value that exceeds the normally accepted 2 Gy tolerance of marrow (45) and is higher than previous studies of marrow dosimetry that have generally used blood sampling to determine dose (Supplemental Appendix 2). This estimate, however, is subject to several limitations as evidenced by the wide variation in absorbed dose (0.01–3.4 Gy/GBq) between patients. This is explained by the heterogeneity in the metastatic burden in the axial skeleton; although we attempted to define the marrow ROI using noninfil-trated bone, this was almost certainly confounded by measuring tumor rather than marrow dose. In patients with extensive metastases, bone marrow distribution is often expanded in the appendicular skeleton and discordant with tumor location (46). Thus, our marrow estimates are almost certainly overestimates as supported by the low incidence of grade 3/4 acute hematologic toxicity (29).

We found a significant correlation between pretherapeutic ^{68}Ga-PSMA PET and estimated dose to tumor, salivary glands, and bone marrow. In the treatment of neuroendocrine tumor, it is reported that the SUV_{max} of ^{68}Ga-DOTATOC PET/CT may predict response to radionuclide therapy (47). In our study, we were unable to determine an SUV_{mean} below which patients are unlikely to respond, though there was a trend for a higher SUV_{mean} to be associated with a PSA response at 12 wk ($P = 0.056$).

In the treatment of neuroendocrine tumors using radiolabeled somatostatin analogs, we have observed that uptake of radionuclide in normal tissues is lower in patients with a high tumor burden because of a tumor-sink effect (48). Recently, Gaertner at el. described reduced uptake of ^{68}Ga-PSMA-11 in salivary glands in patients with high, medium, or low tumor burdens (49). We observed that SUV_{max} and absorbed dose in salivary glands and kidneys decreased significantly with a greater disease burden and a larger physical size. Such findings may be relevant in predicting salivary gland and renal toxicity (50). These data suggest that it may be optimal to deliver higher administered activities to patients with a larger burden of disease and size and, conversely, to reduce activity in patients with a lower disease burden. In contrast to neuroendocrine tumors treated with radiolabeled somatostatin analogs, however, we found no correlation between absorbed dose and renal function.

An association between predicted dose and either therapeutic response or normal-tissue toxicity would provide powerful supportive evidence for the validity and clinical relevance of the dosimetry methods being used. We have observed that an increasing whole-body tumor-absorbed dose occurs in men with a biochemical response, defined by a PSA decline of at least 50%. This parameter accounts for heterogeneity in tumor dose and is perhaps a more relevant estimate of clinical effect than index-lesion dosimetry, noting that the latter did not correlate with a PSA response ($P = 0.09$). However, we also acknowledge the considerable overlap in whole-body tumor dose between individual patients who responded to therapy and those who did not (Fig. 4A), and we would not regard routine dosimetry as mandatory in the clinical application of ^{177}Lu-PSMA therapy.

The relationship between absorbed dose and acute toxicity cannot be evaluated comprehensively in this study, as significant treatment-related adverse events were uncommon (29). We observed no episodes of acute renal toxicity, and the mild xerostomia (all Common Terminology Criteria grade 1) reported by most patients on specific questioning tended to recover with time. The lack of higher-grade xerostomia makes it difficult to assess whether this will be dose-limiting. The results of studies using a higher administered radioactivity and a longer-term follow-up may provide insight into dose-limiting toxicities.

CONCLUSION

In a prospective study reporting the outcomes of ^{177}Lu-PSMA-617 therapy in men with advanced prostate cancer, we observed low normal-organ toxicity with repeated cycles of effective therapy. Mean whole-tumor dose correlates with biochemical response and appears superior to conventional index-lesion dosimetry. Whole-tumor parameters correlated with screening ^{68}Ga-PSMA PET findings. Low doses to salivary glands and kidneys are consistent with the lack of clinically apparent grade 3 or higher toxicity (28). We observed a tumor-sink effect, and this observation may provide a rationale for personalized treatment dosing.

REFERENCES

1. Bostwick DG, Pacelli A, Blute M, Roche P, Murphy GP. Prostate specific membrane antigen expression in prostatic intraepithelial neoplasia and adenocarcinoma: a study of 184 cases. *Cancer.* 1998;82:2256–2261.
2. Kusumi T, Koie T, Tanaka M, et al. Immunohistochemical detection of carcinoma in radical prostatectomy specimens following hormone therapy. *Pathol Int.* 2008;58:687–694.

3. Mannweiler S, Amersdorfer P, Trajanoski S, Terrett JA, King D, Mehes G. Heterogeneity of prostate-specific membrane antigen (PSMA) expression in prostate carcinoma with distant metastasis. *Pathol Oncol Res.* 2009;15:167–172.

4. Ananias HJ, van den Heuvel MC, Helfrich W, de Jong IJ. Expression of the gastrin-releasing peptide receptor, the prostate stem cell antigen and the prostate-specific membrane antigen in lymph node and bone metastases of prostate cancer. *Prostate.* 2009;69:1101–1108.

5. Ross JS, Sheehan CE, Fisher HA, et al. Correlation of primary tumor prostate-specific membrane antigen expression with disease recurrence in prostate cancer. *Clin Cancer Res.* 2003;9:6357–6362.

6. Elsässer-Beile U, Buhler P, Wolf P. Targeted therapies for prostate cancer against the prostate specific membrane antigen. *Curr Drug Targets.* 2009;10:118–125.

7. Tasch J, Gong M, Sadelain M, Heston WD. A unique folate hydrolase, prostate-specific membrane antigen (PSMA): a target for immunotherapy? *Crit Rev Immunol.* 2001;21:249–261.

8. Sokoloff RL, Norton KC, Gasior CL, Marker KM, Grauer LS. A dual-monoclonal sandwich assay for prostate-specific membrane antigen: levels in tissues, seminal fluid and urine. *Prostate.* 2000;43:150–157.

9. Morigi JJ, Stricker PD, van Leeuwen PJ, et al. Prospective comparison of ^{18}F-fluoromethylcholine versus ^{68}Ga-PSMA PET/CT in prostate cancer patients who have rising PSA after curative treatment and are being considered for targeted therapy. *J Nucl Med.* 2015;56:1185–1190.

10. Afshar-Oromieh A, Avtzi E, Giesel FL, et al. The diagnostic value of PET/CT imaging with the ^{68}Ga-labelled PSMA ligand HBED-CC in the diagnosis of recurrent prostate cancer. *Eur J Nucl Med Mol Imaging.* 2015;42:197–209.

11. Maurer T, Gschwend JE, Rauscher I, et al. Diagnostic efficacy of ^{68}gallium-PSMA positron emission tomography compared to conventional imaging for lymph node staging of 130 consecutive patients with intermediate to high risk prostate cancer. *J Urol.* 2016;195:1436–1443.

12. Budäus L, Leyh-Bannurah SR, Salomon G, et al. Initial experience of ^{68}Ga-PSMA PET/CT imaging in high-risk prostate cancer patients prior to radical prostatectomy. *Eur Urol.* 2016;69:393–396.

13. Afshar-Oromieh A, Malcher A, Eder M, et al. PET imaging with a [^{68}Ga]gallium-labelled PSMA ligand for the diagnosis of prostate cancer: biodistribution in humans and first evaluation of tumour lesions. *Eur J Nucl Med Mol Imaging.* 2013;40:486–495.

14. Pandit-Taskar N, O'Donoghue JA, Ruan S, et al. First-in-human imaging with ^{89}Zr-Df-IAB2M anti-PSMA minibody in patients with metastatic prostate cancer: pharmacokinetics, biodistribution, dosimetry, and lesion uptake. *J Nucl Med.* 2016;57:1858–1864.

15. Zechmann CM, Afshar-Oromieh A, Armor T, et al. Radiation dosimetry and first therapy results with a ^{124}I/^{131}I-labeled small molecule (MIP-1095) targeting PSMA for prostate cancer therapy. *Eur J Nucl Med Mol Imaging.* 2014;41:1280–1292.

16. Ahmadzadehfar H, Eppard E, Kurpig S, et al. Therapeutic response and side effects of repeated radioligand therapy with ^{177}Lu-PSMA-DKFZ-617 of castrate-resistant metastatic prostate cancer. *Oncotarget.* 2016;7:12477–12488.

17. Baum RP, Kulkarni HR, Schuchardt C, et al. ^{177}Lu-labeled prostate-specific membrane antigen radioligand therapy of metastatic castration-resistant prostate cancer: safety and efficacy. *J Nucl Med.* 2016;57:1006–1013.

18. Heck MM, Retz M, D'Alessandria C, et al. Systemic radioligand therapy with ^{177}Lu labeled prostate specific membrane antigen ligand for imaging and therapy in patients with metastatic castration resistant prostate cancer. *J Urol.* 2016;196:382–391.

19. Tagawa ST, Milowsky MI, Morris M, et al. Phase II study of lutetium-177-labeled anti-prostate-specific membrane antigen monoclonal antibody J591 for metastatic castration-resistant prostate cancer. *Clin Cancer Res.* 2013;19:5182–5191.

20. Rahbar K, Ahmadzadehfar H, Kratochwil C, et al. German multicenter study investigating ^{177}Lu-PSMA-617 radioligand therapy in advanced prostate cancer patients. *J Nucl Med.* 2017;58:85–90.

21. Kratochwil C, Bruchertseifer F, Giesel FL, et al. ^{225}Ac-PSMA-617 for PSMA-targeted alpha-radiation therapy of metastatic castration-resistant prostate cancer. *J Nucl Med.* 2016;57:1941–1944.

22. Lütje S, Heskamp S, Cornelissen AS, et al. PSMA ligands for radionuclide imaging and therapy of prostate cancer: clinical status. *Theranostics.* 2015;5:1388–1401.

23. Hohberg M, Eschner W, Schmidt M, et al. Lacrimal glands may represent organs at risk for radionuclide therapy of prostate cancer with [^{177}Lu]DKFZ-PSMA-617. *Mol Imaging Biol.* 2016;18:437–445.

24. Delker A, Fendler WP, Kratochwil C, et al. Dosimetry for ^{177}Lu-DKFZ-PSMA-617: a new radiopharmaceutical for the treatment of metastatic prostate cancer. *Eur J Nucl Med Mol Imaging.* 2016;43:42–51.

25. Kabasakal L, AbuQbeitah M, Aygun A, et al. Pre-therapeutic dosimetry of normal organs and tissues of ^{177}Lu-PSMA-617 prostate-specific membrane antigen (PSMA) inhibitor in patients with castration-resistant prostate cancer. *Eur J Nucl Med Mol Imaging.* 2015;42:1976–1983.

26. Okamoto S, Thieme A, Allmann J, et al. Radiation dosimetry for ^{177}Lu-PSMA I&T in metastatic castration-resistant prostate cancer: absorbed dose in normal organs and tumor lesions. *J Nucl Med.* 2017;58:445–450.

27. Yadav MP, Ballal S, Tripathi M, et al. Post-therapeutic dosimetry of ^{177}Lu-DKFZ-PSMA-617 in the treatment of patients with metastatic castration-resistant prostate cancer. *Nucl Med Commun.* 2017;38:91–98.

28. Fendler WP, Kratochwil C, Ahmadzadehfar H, et al. ^{177}Lu-PSMA-617 therapy, dosimetry and follow-up in patients with metastatic castration-resistant prostate cancer [in German]. *Nucl Med (Stuttg).* 2016;55:123–128.

29. Hofman MS, Violet J, Hicks RJ, et al. [^{177}Lu]-PSMA-617 radionuclide treatment in patients with metastatic castration-resistant prostate cancer (LuPSMA trial): a single-centre, single-arm, phase 2 study. *Lancet Oncol.* 2018;19:825–833.

30. Jackson PA, Beauregard JM, Hofman MS, Kron T, Hogg A, Hicks RJ. An automated voxelized dosimetry tool for radionuclide therapy based on serial quantitative SPECT/CT imaging. *Med Phys.* 2013;40:112503.

31. Beauregard JM, Hofman MS, Pereira JM, Eu P, Hicks RJ. Quantitative ^{177}Lu SPECT (QSPECT) imaging using a commercially available SPECT/CT system. *Cancer Imaging.* 2011;11:56–66.

32. Klein S, Staring M, Pluim JP. Evaluation of optimization methods for nonrigid medical image registration using mutual information and B-splines. *IEEE Trans Image Process.* 2007;16:2879–2890.

33. Jan S, Benoit D, Becheva E, et al. GATE V6: a major enhancement of the GATE simulation platform enabling modelling of CT and radiotherapy. *Phys Med Biol.* 2011;56:881–901.

34. Hindorf C, Glatting G, Chiesa C, Linden O, Flux G. EANM dosimetry committee guidelines for bone marrow and whole-body dosimetry. *Eur J Nucl Med Mol Imaging.* 2010;37:1238–1250.

35. Siegel JA, Thomas SR, Stubbs JB, et al. MIRD pamphlet no. 16: techniques for quantitative radiopharmaceutical biodistribution data acquisition and analysis for use in human radiation dose estimates. *J Nucl Med.* 1999;40(suppl):37S–61S.

36. Stabin MG, Sparks RB, Crowe E. OLINDA/EXM: the second-generation personal computer software for internal dose assessment in nuclear medicine. *J Nucl Med.* 2005;46:1023–1027.

37. Garkavij M, Nickel M, Sjogreen-Gleisner K, et al. ^{177}Lu-[DOTA0,Tyr3] octreotate therapy in patients with disseminated neuroendocrine tumors: analysis of dosimetry with impact on future therapeutic strategy. *Cancer.* 2010;116:1084–1092.

38. Sandström M, Garske U, Granberg D, Sundin A, Lundqvist H. Individualized dosimetry in patients undergoing therapy with ^{177}Lu-DOTA-D-Phe^1-Tyr^3-octreotate. *Eur J Nucl Med Mol Imaging.* 2010;37:212–225.

39. Ljungberg M, Sjogreen-Gleisner K. The accuracy of absorbed dose estimates in tumours determined by quantitative SPECT: a Monte Carlo study. *Acta Oncol.* 2011;50:981–989.

40. Dawson LA, Kavanagh BD, Paulino AC, et al. Radiation-associated kidney injury. *Int J Radiat Oncol Biol Phys.* 2010;76(suppl):S108–S115.

41. Bhandare N, Moiseenko V, Song WY, Morris CG, Bhatti MT, Mendenhall WM. Severe dry eye syndrome after radiotherapy for head-and-neck tumors. *Int J Radiat Oncol Biol Phys.* 2012;82:1501–1508.

42. Deasy JO, Moiseenko V, Marks L, Chao KS, Nam J, Eisbruch A. Radiotherapy dose-volume effects on salivary gland function. *Int J Radiat Oncol Biol Phys.* 2010;76(suppl):S58–S63.

43. Bergsma H, Konijnenberg MW, van der Zwan WA, et al. Nephrotoxicity after PRRT with ^{177}Lu-DOTA-octreotate. *Eur J Nucl Med Mol Imaging.* 2016;43:1802–1811.

44. Dale RG. Dose-rate effects in targeted radiotherapy. *Phys Med Biol.* 1996;41:1871–1884.

45. Lassmann M, Hanscheid H, Chiesa C, Hindorf C, Flux G, Luster M. EANM Dosimetry Committee series on standard operational procedures for pre-therapeutic dosimetry I: blood and bone marrow dosimetry in differentiated thyroid cancer therapy. *Eur J Nucl Med Mol Imaging.* 2008;35:1405–1412.

46. Hofman M, Segard T, Khan Z, Seymour J, Hicks R. Clinical utility of ^{18}F-fluoro-L-thymidine (FLT) PET to evaluate bone marrow distribution and proliferation in patients with haematopoietic dysfunction. *J Nucl Med.* 2012;53:538.

47. Kratochwil C, Stefanova M, Mavriopoulou E, et al. SUV of [^{68}Ga]DOTATOC-PET/CT predicts response probability of PRRT in neuroendocrine tumors. *Mol Imaging Biol.* 2015;17:313–318.

48. Beauregard JM, Hofman MS, Kong G, Hicks RJ. The tumour sink effect on the biodistribution of ^{68}Ga-DOTA-octreotate: implications for peptide receptor radionuclide therapy. *Eur J Nucl Med Mol Imaging.* 2012;39:50–56.

49. Gaertner FC, Halabi K, Ahmadzadehfar H, et al. Uptake of PSMA-ligands in normal tissues is dependent on tumor load in patients with prostate cancer. *Oncotarget.* 2017;8:55094–55103.

50. Sabet A, Ezziddin K, Pape UF, et al. Accurate assessment of long-term nephrotoxicity after peptide receptor radionuclide therapy with ^{177}Lu-octreotate. *Eur J Nucl Med Mol Imaging.* 2014;41:505–510.